NeuroImage: Clinical 12 (2016) 785–795

Contents lists available at ScienceDirect

NeuroImage: Clinical

journal homepage: www.elsevier.com/locate/ynicl

Prediction of long-term memory scores in MCI based on resting-state fMRI

Djalel-Eddine Meskaldji[a,b,c,*], Maria Giulia Preti[a,b], Thomas AW Bolton[a,b], Marie-Louise Montandon[d], Cristelle Rodriguez[e], Stephan Morgenthaler[c], Panteleimon Giannakopoulos[e], Sven Haller[f,g,h,i], Dimitri Van De Ville[a,b]

[a] Institute of Bioengineering, Ecole Polytechnique Fédérale de Lausanne (EPFL), Lausanne, Switzerland
[b] Department of Radiology and Medical Informatics, University of Geneva, Geneva, Switzerland
[c] Institute of Mathematics, Ecole Polytechnique Fédérale de Lausanne (EPFL), Lausanne, Switzerland
[d] Divisions of Diagnostic and Interventional Neuroradiology, Geneva University Hospitals, Geneva, Switzerland
[e] Department of Psychiatry, University of Geneva, Switzerland
[f] Affidea CDRC – Centre Diagnostique Radiologique de Carouge, Switzerland
[g] Department of Surgical Sciences, Radiology, Uppsala University, Uppsala, Sweden
[h] Department of Neuroradiology, University Hospital Freiburg, Germany
[i] Faculty of Medicine of the University of Geneva, Switzerland

ARTICLE INFO

Article history:
Received 22 June 2016
Received in revised form 16 September 2016
Accepted 6 October 2016
Available online 11 October 2016

Keywords:
Functional brain connectivity
Cross-validation partial least square regression
Extreme value modeling
Long term memory
Mild cognitive impairment
Medial temporal lobe

ABSTRACT

Resting-state functional MRI (rs-fMRI) opens a window on large-scale organization of brain function. However, establishing relationships between resting-state brain activity and cognitive or clinical scores is still a difficult task, in particular in terms of prediction as would be meaningful for clinical applications such as early diagnosis of Alzheimer's disease. In this work, we employed partial least square regression under cross-validation scheme to predict episodic memory performance from functional connectivity (FC) patterns in a set of fifty-five MCI subjects for whom rs-fMRI acquisition and neuropsychological evaluation was carried out. We show that a newly introduced FC measure capturing the moments of anti-correlation between brain areas, discordance, contains key information to predict long-term memory scores in MCI patients, and performs better than standard measures of correlation to do so. Our results highlighted that stronger discordance within default mode network (DMN) areas, as well as across DMN, attentional and limbic networks, favor episodic memory performance in MCI.

1. Introduction

Large-scale brain organization can be studied based on resting-state functional magnetic resonance imaging (rs-fMRI) data. Functional connectivity (FC) based on rs-fMRI aims at describing spontaneous fluctuations of brain activity as measured by means of the blood oxygenation level dependent (BOLD) contrast. FC between a pair of brain regions is defined as the statistical interdependence between their BOLD time-courses (Friston et al., 1995). Before assessing FC, fMRI signals are preprocessed to remove data acquisition artifacts and other non-desirable confounds. Then, given an anatomical segmentation of the brain cortex, voxel-wise BOLD signals are averaged within each region, yielding a single time-course per region of interest (ROI). In conventional analysis, Pearson correlation coefficient between regionally averaged fMRI time-courses is used as a measure of FC between the regions. The correlation values between all pairs of regions are included in the FC matrix, also referred to as the *functional connectome*, representing the whole-brain connectivity pattern, a complex network that allows in-depth quantitative analysis of brain topology organization (Bullmore and Sporns, 2009; Fornito et al., 2013; Meskaldji et al., 2013; Sporns, 2011).

From a clinical perspective, the potential of FC in depicting functional alterations of resting-state networks was assessed in many neurological disorders (see Fox and Greicius, 2010, for a review), including Alzheimer's disease (AD) and mild cognitive impairment (MCI) (Bai et al., 2008; Li and et al., 2009; Qi et al., 2010; Sorg et al., 2007).

Being considered an intermediate phase between normal aging and dementia (often AD), MCI is characterized by a deficit in at least

* Corresponding author at: Institute of Bioengineering, Ecole Polytechnique Fédérale de Lausanne (EPFL), Lausanne, Switzerland.
E-mail address: djalel.meskaldji@epfl.ch (D. Meskaldji).

http://dx.doi.org/10.1016/j.nicl.2016.10.004

one cognitive domain, without repercussions in daily life (Petersen, 2004). A thorough understanding of the brain functional processes accompanying this condition could be of importance to both MCI diagnosis and to allow early administration of AD drugs under development.

The potential role of fMRI in the early detection of MCI appears particularly promising today, given that the BOLD signal could detect early MCI synaptic dysfunction before the occurrence of structural damage such as cortical volume loss (Terry et al., 2015). Previous resting-state FC studies attempted to define MCI-related alterations, but results appear not fully consistent across studies, most likely due to the use of different methodological approaches and to the heterogeneity of the considered MCI populations. The analysis is often limited to a priori selected regions (Agosta et al., 2012; Bai et al., 2012, 2009; Binnewijzend et al., 2012; Cai et al., 2015; Jin et al., 2012; Liang et al., 2011; Qi et al., 2010; Sorg et al., 2007; Wang et al., 2012a,b, 2011; Yue et al., 2015; Zhang et al., 2015b), and only for a few cases extended to the whole brain (Bai et al., 2008; Chen et al., 2011; Yao et al., 2010; Zhang et al., 2015a). Further more, most of the existing FC studies focus on investigating group differences between MCI and age-matched healthy controls, without exploring the associations between imaging and neuropsychological performance within the MCI sample.

Memory deficits, in particular episodic memory, are often one of the predominant symptoms of MCI. Previous task-based fMRI studies allowed to define the episodic memory network alterations accompanying MCI, mainly involving the medial temporal lobe (MTL) (see Terry et al., 2015, for a review). In particular, discrepant hyper- and hypo-activation of the MTL upon episodic memory tasks was reported in the literature (Terry et al., 2015), and its dependency on the severity of the MCI pathology was proposed (Dickerson and Sperling, 2008). A relationship between off-task intrinsic FC alterations and memory performance was already found in elderly controls (Andrews-Hanna et al., 2007; He et al., 2012; Mevel et al., 2013; Onoda et al., 2012; Touroutoglou et al., 2015; Wang et al., 2010a,b; Yamashita et al., 2015). Applying a similar analysis to MCI would effectively reveal the brain networks that are altered in this condition.

Only a few previous studies attempted to explore the correlation between resting-state FC and memory scores in MCI (Chen et al., 2011; Jin et al., 2012; Liang et al., 2011; Wang et al., 2012b, 2011; Zhang et al., 2012), but the analysis was restricted to specific areas, either a priori selected or showing FC group differences between MCI subjects and controls.

To the best of our knowledge, cross-validated prediction models able to successfully correlate FC changes to memory decline within a group of MCI patients are not present in previous literature. Doing that based on conventional FC measures appears difficult; in fact, Pearson correlation is limited in terms of robustness, and previous studies already attempted to propose alternative FC measures, e.g., involving non-Gaussian methods (Spearman non-parametric correlation, mutual information (Hlinka et al., 2011)). Recent interest in exploring dynamic FC measures (Allen et al., 2014; Karahanoğlu and Van De Ville, 2015; Leonardi et al., 2013) shed light into the need to consider the dynamic aspects of FC to provide a complete picture of functional network organization. The main motivation behind considering dynamics is non-stationarity of brain FC, which cannot be captured with conventional averaging operators such as Pearson correlation when it is computed for the entire time acquisition. Switching between task positive and task negative is also another non-stationarity aspect of brain FC, for which anti-correlations are not considered as a brain dysfunction, but an indication of performance. However, negative correlations are often ignored in brain FC studies, without sufficient justification, while it could contain pertinent information about brain function and performance. This work attempts to show that anti-correlation between fMRI time courses may contain meaningful information in respect to brain activation facing cognitive challenge. To this aim, we use two recently introduced FC measures, accordance and discordance (Meskaldji et al., 2015b), which disentangle the information contained in the traditional Pearson correlation into two complementary metrics in a robust way. These new measures have been shown to bring more consistency and sensitivity in group comparison studies (Meskaldji et al., 2015a). In this work, we show that these two measures bring more predictive performance of individual cognitive scores. Employing a partial least square regression (PLSR) framework, we evaluated the extent to which large-scale FC based on those measures is able to predict individual memory performance in subjects with MCI.

Prediction performance as assessed by correlation between actual and predicted memory scores was $r = 0.64$ using discordance, outperforming Pearson correlation and accordance ($r = 0.53$ and $r = 0.56$, respectively). Results put forward the importance of discordance between default mode network (DMN) nodes, and between DMN, attentional and limbic brain networks, in favoring episodic memory performance in MCI individuals.

2. Methods

2.1. Subjects

Fifty-five subjects diagnosed with MCI (mean age 74.33 ± 6.10, 34 males and 21 females, see Table 1) were included in this study. After formal approval by the local Ethics Committee, informed written consent was obtained from all participants. All subjects had normal or corrected-to-normal visual acuity, and none reported a history of major medical disorders (neoplasm or cardiac illness), sustained head injury, neurologic or psychiatric disorders, alcohol or drug abuse. Subjects with regular use of neuroleptics, antidepressants, mood stabilizers, anticonvulsant drugs, or psycho-stimulants were excluded. All participants underwent the following neuropsychological assessment. We confirmed the MCI status with a shortened test battery including the Mini-Mental State Examination (MMSE) (Folstein et al., 1975), the Hospital Anxiety and Depression Scale (HAD) (Zigmond et al., 1983) and the Lawton's instrumental activities of daily living(IADL) (Barberger-Gateau et al., 1992). Cognitive assessment included attention (Trail Making Test A; Reitan, 1958), verbal working memory (Digit Span Forward; Millis et al., 1999), verbal episodic memory (RI-48 Cued Recall Test, Adam et al., 2007), CERAD 10-word List Delayed Recall Test (Consortium to Establish a Registry for Alzheimer's Disease; Welsh et al., 1994) and RL/RI-16 Free and Cued Remaining Test (Van der Linden and Adam, S., 2004), executive functions (Trail Making Test B; Reitan, 1958, and Phonemic Verbal Fluency test; Cardebat et al., 1989), language (Boston Naming; Kaplan and Goodglass, W. S., 1983), and constructional praxis (CERAD figures copy, Welsh et al., 1994). All individuals were also evaluated with the Clinical Dementia Rating scale (CDR) (Hughes et al., 1982). In agreement with the criteria of Petersen (2004), participants with a CDR score of 0.5 but no dementia and a score more than 1.5 standard deviations below the age-appropriate mean in any of the previously mentioned tests were confirmed to have MCI.

Table 1
Summary of demographics and diagnostic data of MCI subjects.

	Age	MMSE	HAD	CERAD-10
All	74.33 ± 6.10	26.78 ± 2.17	7.17 ± 4.49	5.04 ± 2.25
Male	74.14 ± 5.63	27.12 ± 2.13	7.58 ± 4.55	5.35 ± 1.86
Female	74.62 ± 6.93	26.24 ± 2.17	6.47 ± 4.41	4.52 ± 2.75

2.2. MRI acquisitions

The following acquisitions were performed for all participants on an MR 3T scanner (TRIO, Siemens medical systems, Erlangen, Germany): 1) 3D T1-weighted image: voxel size 1 mm^3 isotropic, 256 × 256 × 176 matrix, TE = 2.27 ms, TR = 2300 ms; 2) multi-echo echo-planar imaging (EPI) covering the entire brain, 74 × 74 × 45 matrix, voxel size 3 mm^3 isotropic, TE = 30 ms, TR = 3000 ms, 180 repetitions for 9 min duration. Simultaneously, a carbon dioxide (CO_2) challenge was administered via a nasal canula in a concentration of 7% mixed in synthetic air, following a block-based paradigm of 1 min OFF, 2 min ON, 2 min OFF, 2 min ON, 2 min OFF. Subjects were asked to breathe normally through the nose and to lie still keeping their eyes closed without thinking at something particular, following the standard resting-state acquisition practice (Fox and Raichle, 2007). The rationale is that the CO_2 challenge would allow assessing neuronal and vascular contributions using a single MR sequence. In the current paper, we only regressed-out the (slow) CO_2 challenge and analyzed the remaining residual time-course as regular resting-state data.

In future work, we will address the potential of using the CO_2 challenge to evaluate the cerebrovascular reserve (CVR), which could be an additional parameter to further increase accuracy and robustness of MR-based diagnosis of cognitive decline. The CO_2 induces a vasodilation, which is a measure of the CVR across the brain. Due to the auto-regulation of the brain, we can assume that first the CVR should be depleted, before the auto regulation is exhausted resulting in a reduction of baseline perfusion (e.g. measured in arterial spin labeling (ASL)). This means that in principle, the CO_2 assessed CVR should be an earlier and more sensitive marker compared to baseline perfusion assessed in ASL.

2.3. Functional MRI preprocessing

The functional volumes were preprocessed using in-house MATLAB scripts including functions from SPM8 DPARSF (Chao-Gan and Yu-Feng, 2010) and IBASPM toolboxes (Aleman-Gomez et al., 2006). Functional images were first spatially realigned to the mean volume and then spatially smoothed by convolution with a Gaussian kernel (8 mm FWHM). A previously published pipeline (Richiardi et al., 2011a, 2012) was used to assess FC. The high-resolution T1 image was linearly registered to the mean functional volume (SPM8 coregistration) and tissue maps (white matter, gray matter, cerebrospinal fluid) were obtained by segmentation of the T1 image with SPM8's New Segment algorithm. The gray matter of every subject was then parcellated into 90 cortical and subcortical regions (AAL atlas; Tzourio-Mazoyer et al., 2002) using a modified version of the IBASPM toolbox. Each parcellation was finally mapped back onto the native resolution of the functional images, yielding the subject-specific functional atlas used later on in the analysis.

The fMRI voxel time-courses were detrended and nuisance variables were regressed out using the DPARSF toolbox (6 head motion parameters, average cerebrospinal fluid and white matter signal from segmentation masks mapped to fMRI resolution). A CO_2 challenge regressor was defined (Richiardi et al., 2015) and regressed out, in order to exclude the effect of the administrated CO_2 from the functional connectivity estimation. Statistical testing showed a negligible Cohen's d effect between with and without CO_2 parts of the time courses. Then, the preprocessed voxel time-courses were spatially averaged within the cortical regions of the functional atlas, yielding 88 regional time-courses (bilateral Pallidum was discarded due to ventral signal dropout). These were eventually band-pass filtered ([0.01–0.15 Hz]), to limit the analysis at the resting-state frequency range (frequencies contributing to FC in the cerebral cortex in resting-state data), and z-scored.

2.4. Functional connectivity estimation

FC should reflect activation in individual brain ROIs. Tagliazucchi et al. (2012) modeled the fMRI signals as a point process by considering its extreme values. However, FC should also reflect how much pairs of ROIs are activated or deactivated at the same time. Recently, Meskaldji et al. (2015a,b) proposed a robust, consistent and yet exhaustive FC estimator based on extreme values. This estimator measures how much two regions are co-activated (co-deactivated) and how much they are not. Specifically, for each pair of regions, two measures are estimated: (1) the accordance, which measures how much two brain ROIs are co-activated and co-deactivated at the same time (co-activation or co-deactivation), and (2) the discordance, which measures the amount of activation-deactivation (no-co-activation and no-co-deactivation) of a pair of time-courses. Fig. 1 illustrates some of the concepts introduced in this section.

This estimator disentangles between parts of the entire time-course that give positive correlation and those parts that give negative correlation (anti-correlation), and hence, reflects non-stationarity features of spontaneous fluctuations of the brain activity.

Formally, let $\mathbf{Z}^T = \mathbf{z_1}, \mathbf{z_2}, \ldots, \mathbf{z_N}$ be the robustly normalized fMRI signals (by subtracting the median and dividing by the median absolute deviation of each time course (Hoaglin et al., 1983)), with $\mathbf{z}_i = z_1^{(i)}, \ldots, z_T^{(i)} \in \mathbb{R}^T$, where N is the number of ROIs and T is the total acquisition time.

In order to keep only significant activations or deactivations of the corresponding brain ROIs, only extreme events of the observed time-courses are considered, that is, each time-course $\mathbf{z}_i, i = 1, \ldots, N$, is compared to a positive and a negative threshold based on a predefined quantile $q = 0.8$. Larger thresholds give more sparse connectivity, while smaller thresholds give non-robust FC estimation (Meskaldji et al., 2015b). The chosen value is close to the one used in Tagliazucchi et al. (2012) ($q \approx 0.84$). We set for each vector $\mathbf{z}$, the thresholded vector z^u such that for all $t \in \{1, \ldots, T\}$: $z_t^u = 0$ if $z_t < u$ and $z_t^u = 1$ otherwise. Similarly, z^l is derived from the vector $\mathbf{z}$ such that for all $t \in \{1, \ldots, T\}$: $z_t^l = 0$ if $z_t > l$ and $z_t^l = -1$ otherwise. The robust normalization and the binarization reduce the influence of very high extremes that might be fMRI time-series artifacts. In the following, we use the notation $\mathbf{z} * \mathbf{z}'$ for the inner product of $\mathbf{z}$ and $\mathbf{z}'$. The accordance $a_{i,j}$ and discordance $d_{i,j}$ values between two ROIs i and j, with corresponding normalized time courses $\mathbf{z}_i$ and $\mathbf{z}_j$, are given by

$$a_{i,j} = \left(\mathbf{z_i^u} * \mathbf{z_j^u} + \mathbf{z_i^l} * \mathbf{z_j^l}\right) / (\sigma_i \sigma_j) \tag{1}$$

$$d_{i,j} = \left(\mathbf{z_i^u} * \mathbf{z_j^l} + \mathbf{z_i^l} * \mathbf{z_j^u}\right) / (\sigma_i \sigma_j), \tag{2}$$

where

$$\sigma_i = \sqrt{(\mathbf{z_i^u} * \mathbf{z_i^u}) + \left(\mathbf{z_i^l} * \mathbf{z_i^l}\right)}. \tag{3}$$

For a given time-course $\mathbf{z}$, the following holds: $a(\mathbf{z}, \mathbf{z}) = 1$, $a(\mathbf{z}, -\mathbf{z}) = 0$ and $d(\mathbf{z}, \mathbf{z}) = 0, d(\mathbf{z}, -\mathbf{z}) = -1$. The discordance value obtained by the algorithm is always negative. However, for ease of interpretation, we use its absolute value from now on. Finally, to study the consistency of FC measures, cross-subject average connectivity matrices were computed for each measure.

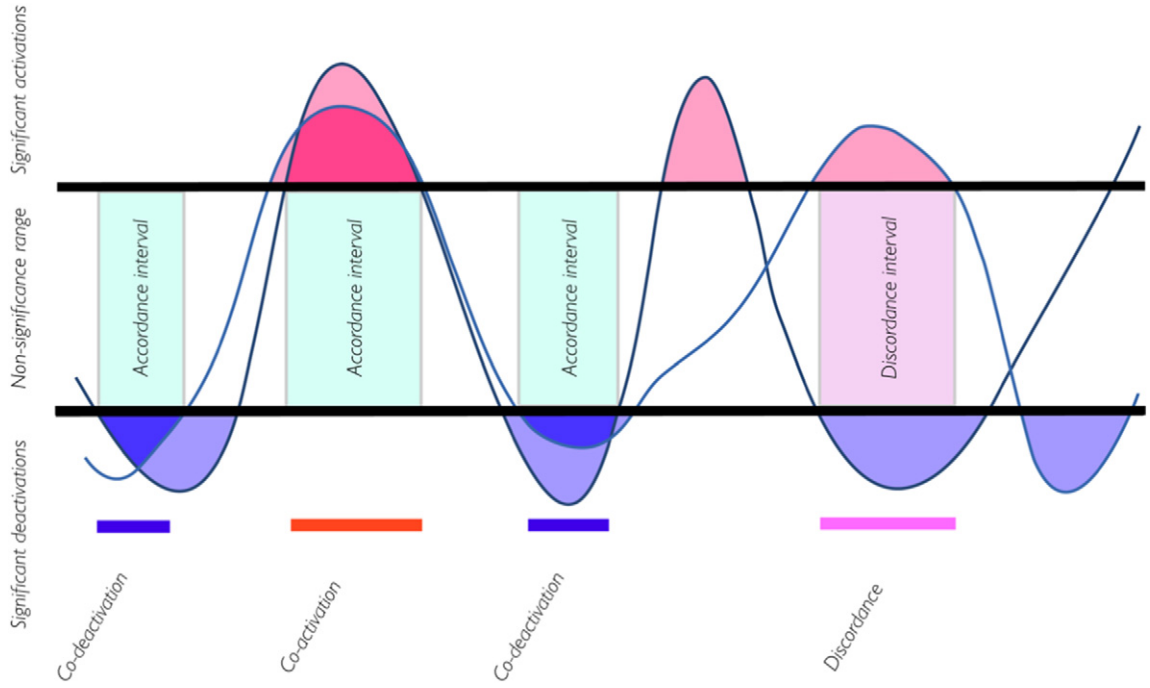

Fig. 1. Illustration of the concepts used in the definition of accordance and discordance FC estimator. The figure shows two normalized time-courses. Only parts above the positive threshold (red parts) and below the negative threshold (blue parts) are considered as significant activations and deactivations, respectively. The overlapping of activation parts represents co-activation, and the overlapping of deactivation parts represents co-deactivation. These parts contribute in computing accordance value. The overlapping of activation parts of one time-course with deactivation parts of the second time-course (purple) contributes in computing discordance values. (For interpretation of the references to color in this figure legend, the reader is referred to the web version of this article.)

2.5. Prediction

As mentioned in the introduction, previous correlation/prediction studies have been focusing on specific regions of the brain known to be related to memory performance. Other studies have first identified connections that differ between MCI subjects and healthy controls and then focused on those. Contrarily, our approach uses the whole set of connections, which might capture interactions that relate to memory performance better than in prior or difference-based subset selection. However, this makes prediction challenging due to the large number of connections. For this reason, we used PLSR to predict the memory scores (MSs), that is, the CERAD 10-word list delayed recall test for episodic memory in MCI subjects.

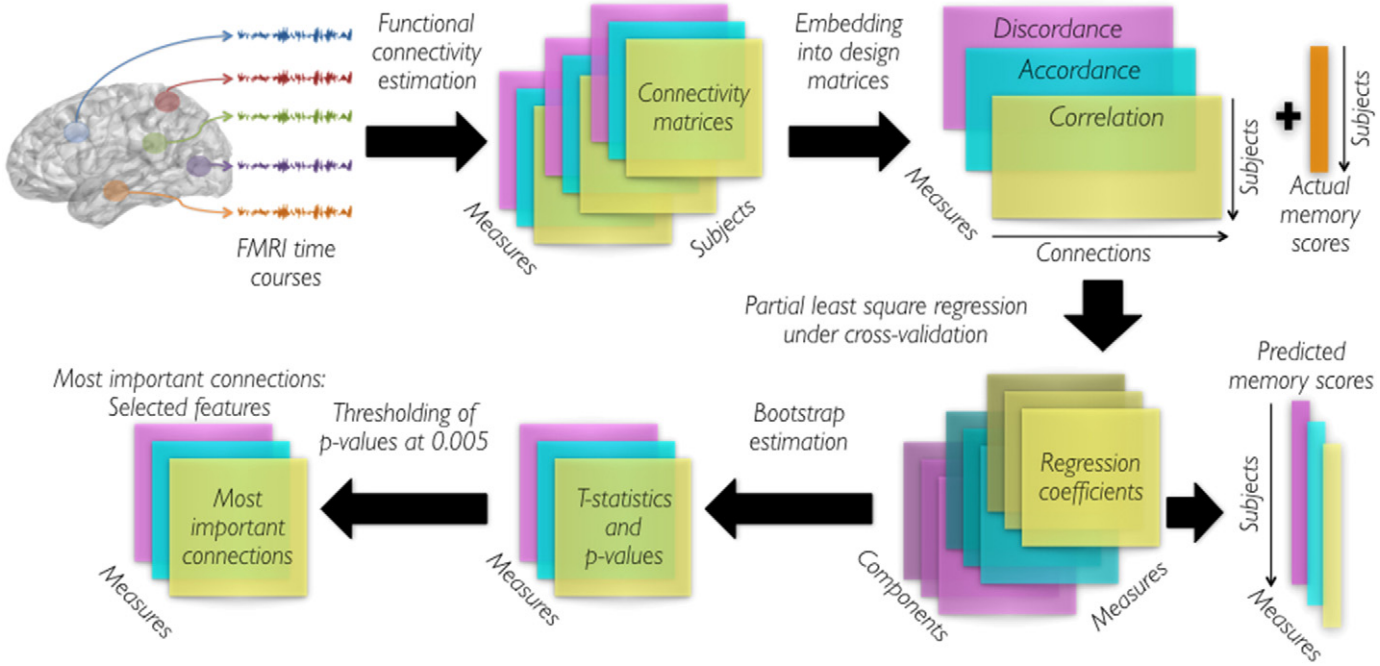

Fig. 2. Processing pipeline to derive prediction models and evaluate their performances.

PLSR is one of the multivariate regression methods that have been widely used in various application fields such as social sciences, bioinformatics and neuroscience (Cramer et al., 1988;McIntosh et al., 1996;Nguyen and Rocke, 2002). The reason is that PLSR could be used as an alternative to linear regression in situations where the number of predictors is relatively large compared to the number of available samples. Instead of projecting the response vector into the space spanned by the co-variables, PLSR projects both the response and the co-variables into a new space formed by latent variables.

PLSR benefits from dimensionality reduction by using only few loading components.

To construct the design matrix **X**, for each measure, we embed the $N(N-1)/2 = 88(88-1)/2 = 3828$ connectivity values of each subject in a vector, i.e., each column of the **X** matrix corresponds to a connection in the functional connectome, and each line of the **X** matrix corresponds to one subject. Hence, the **X** matrix for each measure (Pearson correlation, accordance or discordance) is of size $n \times N(N-1)/2 = 55 \times 3828$, where n is the number of subjects. Then, PLSR is performed to derive regression coefficients for predicting the MSs from the connectivity measures **X**. For more details, see Appendix A.

PLSR predictive performance is evaluated by 1) estimating the correlation between the actual and the predicted MSs, and 2) by estimating the prediction R^2, which is given by

$$R^2 = 1 - \frac{\sum_{k=1}^{n} \left(\hat{Y}_k - Y_k\right)^2}{\sum_{k=1}^{n} \left(Y_k - \bar{Y}\right)^2},$$

where $\hat{Y}_k$ is the predicted score for subject k, and $\bar{Y}$ is the mean of actual scores. It is evident that the more the number of variables/components in the model, the better (closer to one) is the R-square. Even if we randomize subject scores, we still obtain good performances of regression. This problem is known as overfitting. In order to avoid it, the prediction is realized under cross-validation (CV) scheme. We trained a PLSR model by excluding some subjects from the data. Once the regression coefficients are estimated from the training set, we use them to predict the MSs for the excluded subjects (testing set).

We considered the following CV cases: 1) leave-one-out cross-validation (LOO-CV) (Lachenbruch and Mickey, 1968), in which the testing set consists of one subject only; 2) random (not necessarily independent) 5 folds with possibly different sizes (CV-5-rand); and finally, 3) 5 independent folds with equal size 11 (CV-5-indep). Except for the first case (LOO-CV), there are many possibilities to chose the training set in order to estimate PLS coefficients for the testing set. In all theses cases, we repeated the process 1000 times and we report their summary predictive performance. We compared the PLS performance of the LOO-CV to the one obtained by randomization of subject labels. This affords us to estimate non-parametric permutation test p-values. Note that if we randomize scores, the correlation between actual and LOO-predicted scores is close to zero under cross-validation.

We used bootstrapping to find the optimal number of PLSR components. Because of the non-linearity relationship between memory scores and connectivity measures, the variance of predicted memory scores is reduced compared to the variance of actual scores. Consequently, bearing in mind that the predicted mean scores is the same as the mean of the actual scores, the predicted scores are rescaled around the mean proportionally to the root square of the ratio between the variance of the actual scores and the variance of the predicted scores (see Appendix A). This solution does not affect the ranking of the predicted scores. We integrated this rescaling under the CV framework. For example, in the LOO case, the rescaled

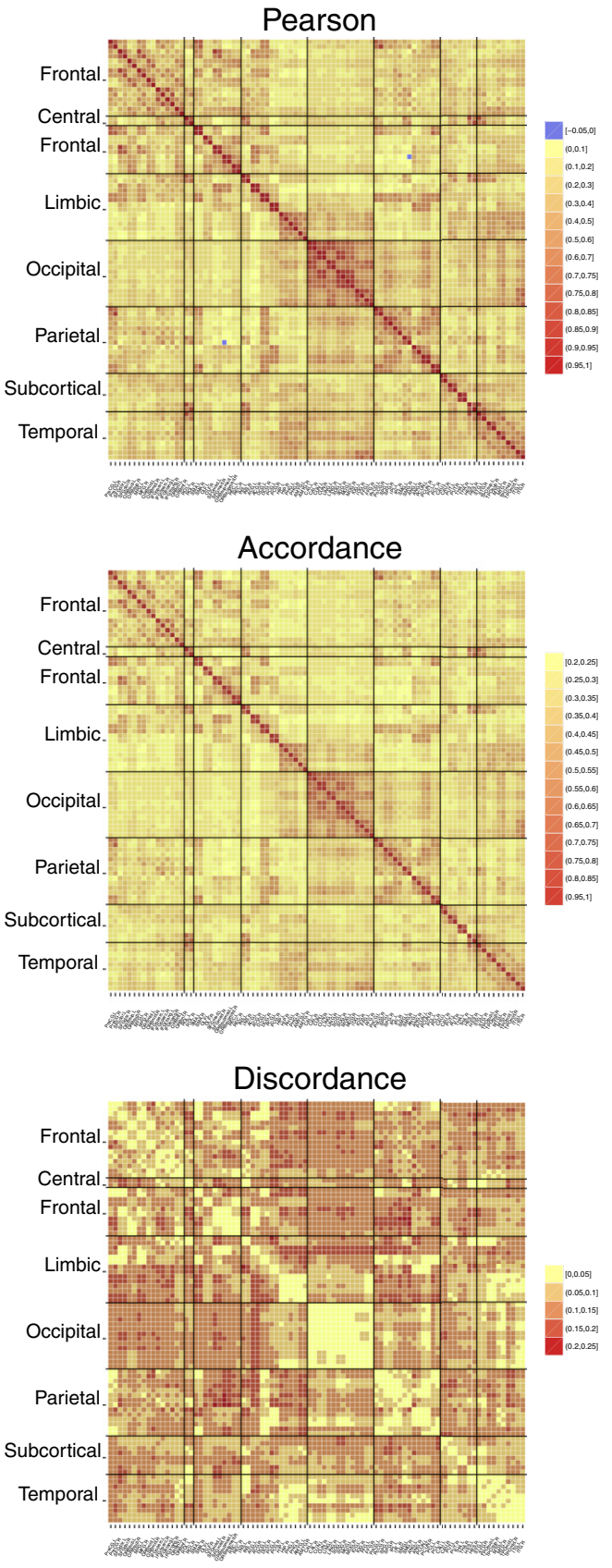

Fig. 3. Mean connectivity matrices (across subjects) corresponding to the Pearson correlation, accordance and discordance measures, respectively.

predicted values are given by

$$\hat{Y}_k = \bar{Y} + (\tilde{Y}_k - \bar{Y})\Big(var(\mathbf{Y})/var(\tilde{\mathbf{Y}}_{-k})\Big)^{1/2},$$

where $\tilde{Y}_k$ is the PLS estimated score and $\tilde{\mathbf{Y}}_{-k}$ is the vector of all estimated PLS scores except $\tilde{Y}_k$.

We also used bootstrapping to estimate t-scores that assess the importance of each connection in the PLSR model in the LOO case. The corresponding p-values are thresholded at level 0.005 to highlight the subset of relevant connections related to long-term memory.

All the steps described above are performed for each measure (Pearson correlation, accordance and discordance). Fig. 2 summarizes the undertaken steps of the pipeline.

3. Results

3.1. FC measures consistency

Fig. 3 illustrates the average Pearson correlation, accordance and discordance connectivity matrices across all MCI subjects. These average matrices reflect the consistency of the connectivity pattern between subjects. It is observable that the average Pearson correlation matrix shows much stronger positive than negative values, ranging between −0.05 and 1. The positive pattern of average Pearson correlation is replicated by the average accordance, which catches the co-activations and co-deactivations of signals. The narrower range of negative correlations is instead captured and amplified by discordance. By having two distinct measures for the depiction of positive and negative correlation (respectively, accordance and discordance), we can plot both with positive sign (high values of discordance, which would have been negative in correlation, are now displayed as positive).

3.2. Comparison between the three prediction models

Fig. 1 (Supplementary material) shows the root mean squared error of prediction (RMSEP) of the three PLSR models built on Pearson correlation, accordance and discordance data, respectively. According to these plots, the optimal number of components is 5 for all measures; Pearson correlation, accordance and discordance.

Fig. 4 shows the predicted MSs as obtained by PLSR with the aforementioned number of components under LOO-CV scheme, versus the actual episodic MSs. Among the models, the one based on discordance is the best in terms of correlation between predicted values and actual values (r = 0.64, permutation p = 1e−5), whereas Pearson and accordance yield almost similar performance (r = 0.53, permutation p = 1.23e−3 and r = 0.56, permutation p = 1.9e−4, respectively). The permutation p-values are obtained on the basis of 10^5 permutations. The estimated R^2 shows also better performance for discordance compared to accordance and Pearson correlation. R^2 is 0.26, 0.31 and 0.41 for Pearson, accordance and discordance, respectively. The two other CV schemes give slightly less predictive performance while preserving the advantage of discordance over accordance and of accordance over Pearson correlation (see Supplementary material, Table 1).

Fig. 5 shows the PLSR t-values for the three models estimated with the bootstrapping technique. As for the mean connectivity matrices, a clear resemblance between the correlation and accordance cases is observable (correlation between Pearson based t-statistics and accordance based t-statistics = 0.84, p ≤ 2.2e−16), while a different pattern is found for discordance (correlation = 0.04, p = 0.002 with accordance t-statistics, and 0.02, p = 0.11 with Pearson t-statistics).

3.3. Most predictive connections

In order to retain the most important connections related to the long-term MS, we thresholded the p-values corresponding to PLSR coefficients, at p=0.005. After this thresholding, the three measures (Pearson correlation, accordance and discordance) yielded 14, 26 and 30 most important connections. The different number of selected connections reflects the fact that the PLSR t-maps are more organized and structured in accordance- and discordance-based models than in the Pearson correlation based model. These retained connections are listed in Tables 2, 3 and 4 in the Supplementary material. Connections of discordance model are also represented in brain graphs, in Fig. 6 (connections of Pearson and accordance based models are represented in brain graphs in Fig. 2 in the Supplementary material). In the brain maps, orange connections contribute positively to the MS (positive regression coefficient in the PLSR model), while blue connections contribute negatively to the MS (negative regression coefficient in the PLSR model). We used the Brain Net Viewer tool for the brain maps visualization (Xia et al., 2013).

The prediction models based on Pearson correlation and accordance seem to involve the same regions as network hubs: larger Pearson correlation or accordance measures of middle and inferior frontal gyri with the rest of the brain (positive t-values), and lower values for amygdala (negative t-values) contribute to better memory

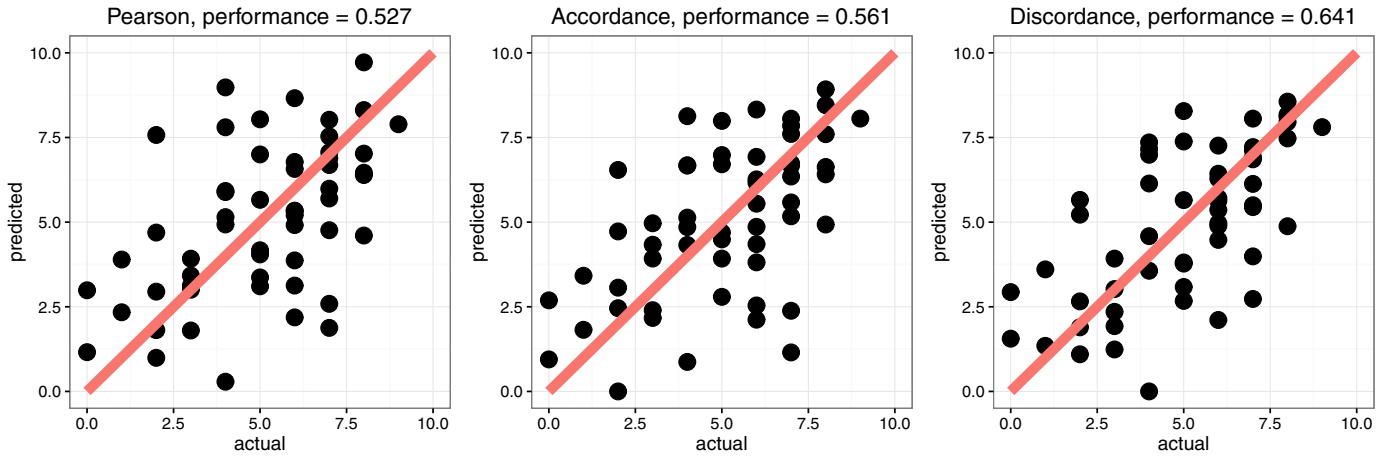

Fig. 4. Predicted vs measured memory scores corresponding to different measures (Pearson correlation, accordance and discordance). Predicted values are obtained by performing LOO PLSR models, in which co-variables are the connectivity values. We also report the correlation between predicted and measured values for each model.

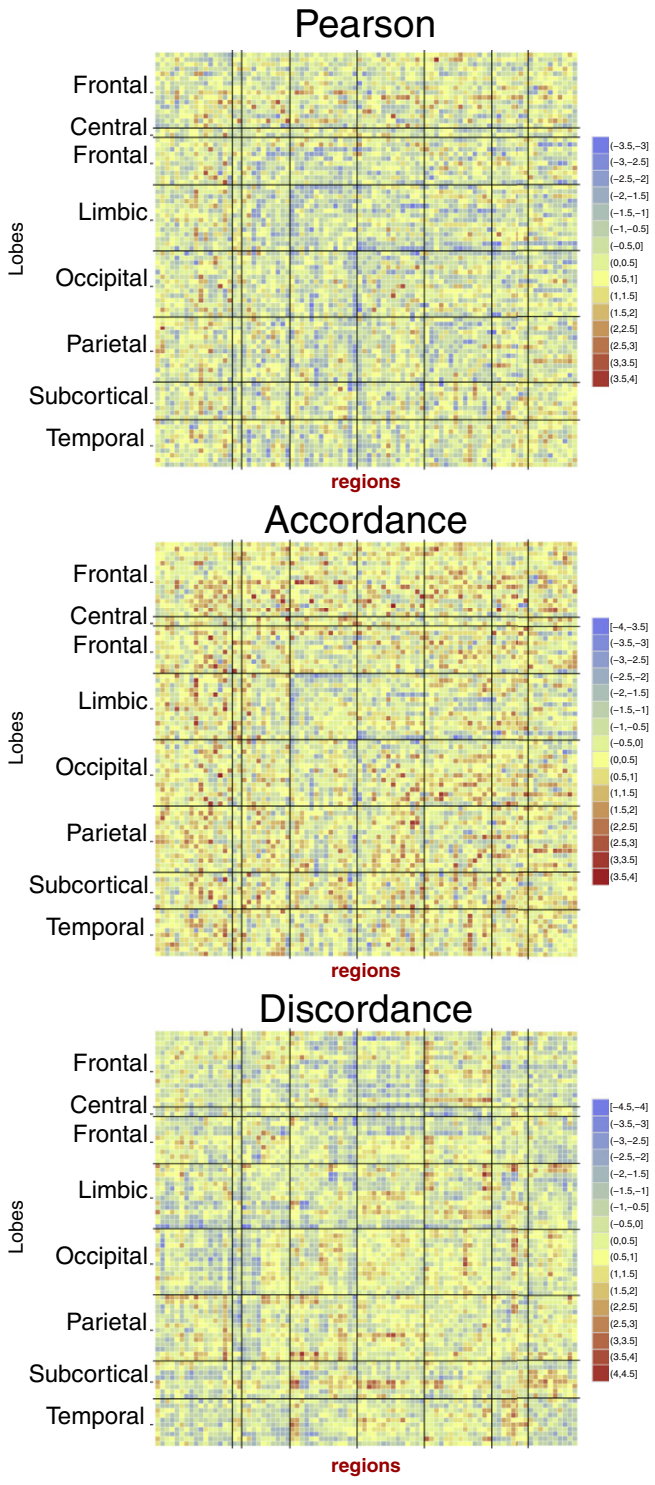

Fig. 5. T-statistic maps corresponding to the coefficients of the PLSR models for the different measures (Pearson correlation, accordance and discordance).

performance. Instead, distinct brain networks appear to be involved in the discordance model, highlighting in particular the role of the DMN (including the hippocampus and temporal regions), the attention network, the limbic system (thalamus, amygdala) and the supplementary motor areas (SMA).

4. Discussion

4.1. Consistent estimation of FC

The newly introduced measures of accordance and discordance represent a robust and exhaustive estimator of FC. It is robust because it only considers significant activations and deactivations, and it is exhaustive because it splits the correlation into two parts: the first one mainly contributing to positive correlation and the second one to negative correlation (i.e., anti-correlation). Accordance captures the common activations or deactivations of brain areas, which are usually seen in the positive values of correlation. Negative values of Pearson correlation also exist, but vary within a narrower range, as pointed out in the mean Pearson correlation matrix in Fig. 3 (positive average Pearson correlation range: [0; 1], negative average Pearson correlation range: [−0.05; 0]). Discordance is able to capture this less often assessed information, which may also be relevant for FC analysis but is usually hidden by Pearson correlation. The use of the same sign for the two measures avoids the problem of having negative values when estimating network topological measures, encountered with correlation-based connectivity matrices (Meskaldji et al., 2015c). Finally, a study of the consistency and sensitivity of FC measures should include the estimation of the intra-class correlation coefficient, which affords an in-depth comparison between the extreme based measures and other FC measures.

4.2. Prediction of memory scores from FC

Compared to most previous works, our analysis was conducted in a whole-brain manner, avoiding initial bias resulting from seed selection. Only a minor subset of studies has attempted to do so, but without reaching a consensus on the connectivity alterations characterizing memory performance in MCI. Furthermore, these studies limited their analysis to group comparison between healthy and MCI individuals. In the present work, we explore a more challenging approach in which we implement a PLSR model able to highlight the subset of relevant connections for the prediction of long-term MSs within a group of MCI patients.

Overall, all measures give good prediction performance despite the heterogeneity of the MCI population. This shows the ability of predicting memory performance from fMRI data, which is promising and a clear indication that rs-fMRI data contains an important amount of information about brain function, organization and synchronization. Although leave one out CV already considers independent sets for validation since each built model is tested on an external or independent data, it suffers from some undesirable features in some cases. However, with our data we show that LOO and k-folds cross-validations have almost the same predictive performances and preserve the ranking of predictive performance (discordance, accordance and Pearson correlation). The small difference could be explained either by the differences in the techniques themselves or by the level of homogeneity of the data (Meskaldji et al., 2016). It is important to bear in mind the possible bias in the prediction caused by the variability of the memory scores, which is one of the limitations of this study. In future investigation, it is recommended to use more accurate estimation of memory performance. This could be obtained, for example, by averaging several test runs. The prediction performance could be improved by using non-linear models to avoid bias in variance estimation under cross-validation as we have encountered in this study. It could be further improved using other meaningful features of brain connectivity such as graph theory measures that characterize topology of brain networks (Richiardi et al., 2011b; Smith et al., 2013). Here again, the combination of accordance and discordance has a conceptual advantage if these two measures are considered separately, especially, in local brain analysis (Meskaldji et al., 2015d).

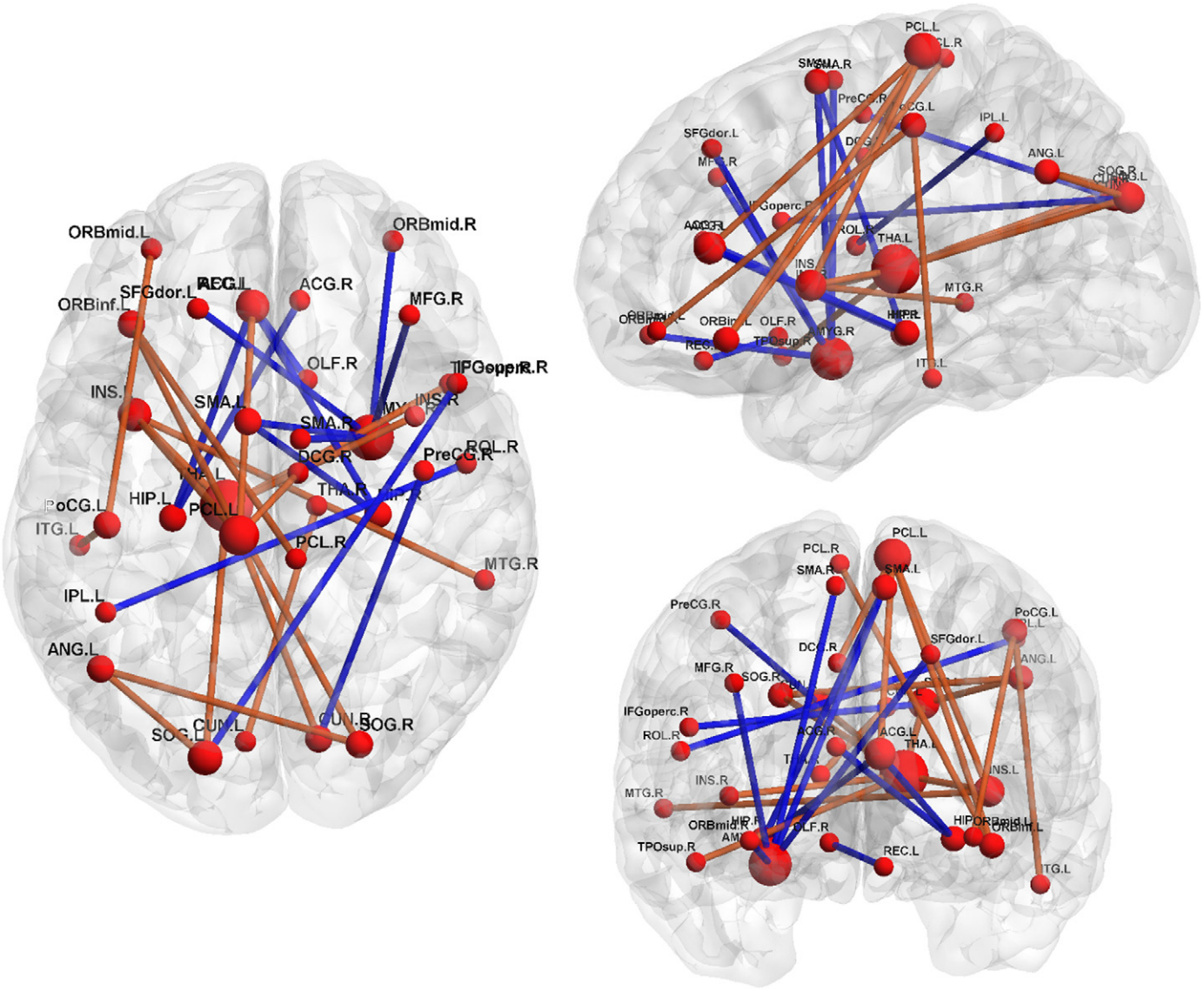

Fig. 6. Significant connections obtained by thresholding p-values (at level 0.005) corresponding to the coefficients of the discordance based model. The connection color represents the sign of the coefficient corresponding to each connection in the PLSR model (orange for positive coefficients and blue for negative coefficients). The node size is proportional to the node degree in the absolute t-map. (For interpretation of the references to color in this figure legend, the reader is referred to the web version of this article.)

Surprisingly, of the three FC measures explored, the discordance based model showed the best performance in terms of correlation between the predicted and the actual MSs (Fig. 4). This finding raises the question about negative correlations that are often ignored, without strong argumentation, while we see clearly that anti-correlation contains meaningful information about memory performance.

4.3. Episodic memory-related networks in MCI: new insights from discordance

The additional networks provided by the discordance model with respect to the usual Pearson correlation analysis included areas from the DMN (right middle frontal gyrus, anterior cingulate cortices, left angular gyrus, bilateral hippocampi and temporal areas), the attention network (right precentral gyrus and bilateral paracentral lobules), additional limbic regions (right amygdala, bilateral thalamus and insula), and bilateral supplementary motor areas (SMA; see Supplementary Table 3). All these systems of areas have been related to healthy-to-MCI changes in past seed-based or whole-brain studies (Sorg et al., 2007; Bai et al., 2009; Qi et al., 2010; Wang et al., 2011; Wang et al., 2012b; Liang et al., 2011; Wang et al., 2012a; Cai et al., 2015; Bai et al., 2008; Wang et al., 2011; Yi et al., 2012; Liu et al., 2012; Yao et al., 2010; Chen et al., 2011; Wee et al., 2012; Wee et al., 2015; Zhang et al., 2015a), even if no specific link to memory performance is drawn in most cases.

Temporal areas, including the hippocampus and medial temporal gyrus, are well-known linked to the memory system and were non-surprisingly found in several previous studies. Here, we can observe that a higher discordance between hippocampal regions and the anterior cingulate cortex (both included as DMN regions) impedes episodic memory performance (blue connections in Fig. 6). This finding appears in line with previous work in which it was shown that the medial temporal lobe formation can dissociate from the canonical DMN in resting-state (Yeo et al., 2011), contributing to a more restricted network that activates upon episodic memory retrieval (Andrews-Hanna, 2012).

At the same time, the anti-correlation between the attentional system (bilateral paracentral and right precentral lobules) and some regions of the DMN (left anterior cingulate cortex, left inferior temporal gyrus), the left insula and the orbitofrontal gyri, goes with better long-term memory performance. These results could reflect a worse capability of the more memory-impaired MCI subjects to synchronously alternate between the task-positive (attentional) and task-negative (default-mode) systems, which squares well with previous findings showing a loss of this inter-network relationship along the progression of Alzheimer's disease (Brier et al., 2012).

Interestingly, the lower discordance of the bilateral SMA with the right amygdala and the hippocampal formation seems to favor memory performance. As the SMA has also been linked to lexical selection (Alario et al., 2006), we can speculate that the anti-correlated behavior of this network with the salience network (amygdala) and memory system (hippocampus) plays a detrimental role in the words-recalling test considered here.

Finally, the thalamus seems to play a relevant role for episodic memory, standing out as the largest hub node in the discordance brain graphs. Specifically, its higher antagonistic interaction with a wide network including temporal, occipital and insular areas favors long term-memory. This finding is in line with recent evidence pointing at the thalamus as a fundamental intermediate region for the communication between different cortical areas (Sherman, 2007, 2016).

5. Conclusion

In this work, we highlight the importance of discordance as an alternative or complementary measure of FC to capture yet under-looked aspects of brain functional interactions. Deploying this measure, inter-individual mnemonic differences could be accurately resolved in a set of MCI subjects, highlighting the importance of anti-correlation both within and across some of the major resting-state brain systems (DMN, attentional, limbic).

Acknowledgments

This work was supported in part by the Swiss National Science Foundation (grant numbers: 200020-144467 and PP00P2-146318), by the Bertarelli Foundation, and by the Center for Biomedical Imaging (CIBM) of the Geneva-Lausanne Universities and the EPFL.

Appendix A. Appendix

In the usual linear regression modeling, the least square solution for

$$\mathbf{Y} = \mathbf{XB} + \mathcal{E} \tag{4}$$

is given by

$$\mathbf{B} = \left(\mathbf{X}^T\mathbf{X}\right)^{-1}\mathbf{X}^T\mathbf{Y}. \tag{5}$$

When the number of parameters is large compared to the number of samples, it happens that $(\mathbf{X}^T\mathbf{X})^{-1}$ is singular, and the solution cannot be evaluated, unless a regularization is applied such as the LASSO method (Tibshirani, 1996). PLSR regression overcomes this singularity by decomposing both **X** and **Y** into orthogonal scores and loadings. The general formulation is given by

$$\mathbf{X} = \mathbf{TP}^T + \mathcal{E}_X \tag{6}$$

$$\mathbf{Y} = \mathbf{UQ}^T + \mathcal{E}_Y, \tag{7}$$

where **T** and **U** are scores, while **P** and **Q** are the loading matrices for **X** and **Y**, respectively. $\mathcal{E}_X$ and $\mathcal{E}_Y$ are independent errors. The scores and the loadings are chosen to explain the maximum variance between **X** and **Y**. PLSR tries to find the directions in **X** that better explain the maximum variance in **Y**. There are many algorithms to solve the PLSR problem. In our application, we used the "pls" (Mevik and Wehrens, 2007) R-package (http://cran.r-project.org). In this package, the choice of the optimal number of components is based on the root mean squared error of prediction (RMSEP). There are two cross-validation estimates of the RMSEP: the ordinary CV estimate, and the bias-corrected CV estimate (Mevik and Cederkvist, 2004; Mevik and Wehrens, 2007). After estimation of the LOO-PLSR models, the importance of connections in the models is assessed using the bootstrapping Jackknife test estimator (Martens and Martens, 2000) also implemented in the "pls" (Mevik and Wehrens, 2007) R-package.

Appendix B. Supplementary data

Supplementary data to this article can be found online at http://dx.doi.org/10.1016/j.nicl.2016.10.004.

References

Adam, S., Van der Linden, M., Ivanoiu, A., Juillerat, A.C., Béchet, S., Salmon, E., 2007. Optimization of encoding specificity for the diagnosis of early ad: the ri-48 task. J. Clin. Exp. Neuropsychol. 29 (5), 477–487.

Agosta, F., Pievani, M., Geroldi, C., Copetti, M., Frisoni, G.B., Filippi, M., 2012. Resting state fMRI in Alzheimer's disease: beyond the default mode network. Neurobiol. Aging 33 (8), 1564–1578.

Alario, F.X., Chainay, H., Lehericy, S., Cohen, L., 2006. The role of the supplementary motor area (SMA) in word production. Brain Res. 1076 (1), 129–143.

Aleman-Gomez, Y., Melie-García, L., Valdés-Hernandez, P., 2006. IBASPM: toolbox for automatic parcellation of brain structures. 12th Annual Meeting of the Organization for Human Brain Mapping. vol. 27.

Allen, E.A., Damaraju, E., Plis, S.M., Erhardt, E.B., Eichele, T., Calhoun, V.D., 2014. Tracking whole-brain connectivity dynamics in the resting state. Cereb. Cortex Bhs352.

Andrews-Hanna, J.R., 2012. The brain's default network and its adaptive role in internal mentation. Neuroscientist 18 (3), 251–270.

Andrews-Hanna, J.R., Snyder, A.Z., Vincent, J.L., Lustig, C., Head, D., Raichle, M.E., Buckner, R.L., 2007. Disruption of large-scale brain systems in advanced aging. Neuron 56 (5), 924–935.

Bai, F., Shi, Y., Yuan, Y., Wang, Y., Yue, C., Teng, Y., Wu, D., Zhang, Z., Jia, J., Zhang, Z., 2012. Altered self-referential network in resting-state amnestic type mild cognitive impairment. Cortex 48 (5), 604–613.

Bai, F., Watson, D.R., Yu, H., Shi, Y., Yuan, Y., Zhang, Z., 2009. Abnormal resting-state functional connectivity of posterior cingulate cortex in amnestic type mild cognitive impairment. Brain Res. 1302, 167–174.

Bai, F., Zhang, Z., Yu, H., Shi, Y., Yuan, Y., Zhu, W., Zhang, X., Qian, Y., 2008. Default--mode network activity distinguishes amnestic type mild cognitive impairment from healthy aging: a combined structural and resting-state functional MRI study. Neurosci. Lett. 438 (1), 111–115.

Barberger-Gateau, P., Commenges, D., Gagnon, M., Letenneur, L., Sauvel, C., Dartigues, J.F., 1992. Instrumental activities of daily living as a screening tool for cognitive impairment and dementia in elderly community dwellers. J. Am. Geriatr. Soc. 40 (11), 1129–1134.

Binnewijzend, M.A., Schoonheim, M.M., Sanz-Arigita, E., Wink, A.M., van der Flier, W.M., Tolboom, N., Adriaanse, S.M., Damoiseaux, J.S., Scheltens, P., van Berckel, B.N., et al. 2012. Resting-state fMRI changes in Alzheimer's disease and mild cognitive impairment. Neurobiol. Aging 33 (9), 2018–2028.

Brier, M.R., Thomas, J.B., Snyder, A.Z., Benzinger, T.L., Zhang, D., Raichle, M.E., Holtzman, D.M., Morris, J.C., Ances, B.M., 2012. Loss of intranetwork and internetwork resting state functional connections with Alzheimer's disease progression. J. Nurs. 32 (26), 8890–8899.

Bullmore, E., Sporns, O., 2009. Complex brain networks: graph theoretical analysis of structural and functional systems. Nat. Rev. Neurosci. 10 (3), 186–198.

Cai, S., Huang, L., Zou, J., Jing, L., Zhai, B., Ji, G., von Deneen, K.M., Ren, J., Ren, A., Initiative, A.D.N., et al. 2015. Changes in thalamic connectivity in the early and late stages of amnestic mild cognitive impairment: a resting-state functional magnetic resonance study from ADNI. PloS one 10 (2).

Cardebat, D., Doyon, B., Puel, M., Goulet, P., Joanette, Y., 1989. Formal and semantic lexical evocation in normal subjects. Performance and dynamics of production as a function of sex, age and educational level. Acta Neurol. Belg. 90 (4), 207–217.

Chao-Gan, Y., Yu-Feng, Z., 2010. DPARSF: a Matlab toolbox for "pipeline" data analysis of resting-state fMRI. Front. Syst. Neurosci. 4.

Chen, G., Ward, B.D., Xie, C., Li, W., Wu, Z., Jones, J.L., Franczak, M., Antuono, P., Li, S.J., 2011. Classification of Alzheimer disease, mild cognitive impairment, and normal cognitive status with large-scale network analysis based on resting-state functional mr imaging. Radiology 259 (1), 213–221.
Cramer, R.D., Patterson, D.E., Bunce, J.D., 1988. Comparative molecular field analysis (CoMFA). 1. Effect of shape on binding of steroids to carrier proteins. J. Am. Chem. Soc. 110 (18), 5959–5967.
Dickerson, B.C., Sperling, R.A., 2008. Functional abnormalities of the medial temporal lobe memory system in mild cognitive impairment and Alzheimer's disease: insights from functional MRI studies. Neuropsychologia 46 (6), 1624–1635.
Folstein, M.F., Folstein, S.E., McHugh, P.R., 1975. "Mini-mental state": a practical method for grading the cognitive state of patients for the clinician. J. Psychiatr. Res. 12 (3), 189–198.
Fornito, A., Zalesky, A., Breakspear, M., 2013. Graph analysis of the human connectome: promise, progress, and pitfalls. Neuroimage 80 (0), 426–444. Mapping the Connectome.
Fox, M.D., Greicius, M., 2010. Clinical applications of resting state functional connectivity. Front. Syst. Neurosci. 4.
Fox, M.D., Raichle, M.E., 2007. Spontaneous fluctuations in brain activity observed with functional magnetic resonance imaging. Nat. Rev. Neurol. 8 (9), 700–711.
Friston, K.J., Holmes, A.P., Worsley, K.J., Poline, J.-P., Frith, C.D., Frackowiak, R.S.J., 1995. Statistical parametric maps in functional imaging: a general linear approach. Hum. Brain Mapp. 2 (4), 189–210.
He, J., Carmichael, O., Fletcher, E., Singh, B., Iosif, A.M., Martinez, O., Reed, B., Yonelinas, A., DeCarli, C., 2012. Influence of functional connectivity and structural MRI measures on episodic memory. Neurobiol. Aging 33 (11), 2612–2620.
Hlinka, J., Paluš, M., Vejmelka, M., Mantini, D., Corbetta, M., 2011. Functional connectivity in resting-state fMRI: is linear correlation sufficient? Neuroimage 54 (3), 2218–2225.
Hoaglin, D.C., Mosteller, F., Tukey, J.W., 1983. Understanding Robust and Exploratory Data Analysis. vol. 3. Wiley, New York.
Hughes, C.P., Berg, L., Danziger, W.L., Coben, L.A., Martin, R.L., 1982. A new clinical scale for the staging of dementia. Br. J. Psychiatry 140 (6), 566–572.
Jin, M., Pelak, V.S., Cordes, D., 2012. Aberrant default mode network in subjects with amnestic mild cognitive impairment using resting-state functional MRI. Magn. Reson. Imaging 30 (1), 48–61.
Kaplan, E.F., Goodglass, H., W. S., 1983. The Boston Naming Test. Lea & Febiger, Philadelphia.
Karahanoğlu, F.I., Van De Ville, D., 2015. Transient brain activity disentangles fMRI resting-state dynamics in terms of spatially and temporally overlapping networks. Nat. Commun. 6.
Lachenbruch, P.A., Mickey, M.R., 1968. Estimation of error rates in discriminant analysis. Technometrics 10 (1), 1–11.
Leonardi, N., Richiardi, J., Gschwind, M., Simioni, S., Annoni, J.M., Schluep, M., Vuilleumier, P., Van De Ville, D., 2013. Principal components of functional connectivity: a new approach to study dynamic brain connectivity during rest. Neuroimage 83, 937–950.
Li, K., et al. 2009. Review on methods for functional brain connectivity detection using fMRI. Comp. Medical Img. Graph. 33, 131–139.
Liang, P., Wang, Z., Yang, Y., Jia, X., Li, K., 2011. Functional disconnection and compensation in mild cognitive impairment: evidence from DLPFC connectivity using resting-state fMRI. PloS one 6 (7), e22153.
Liu, Z., Zhang, Y., Yan, H., Bai, L., Dai, R., Wei, W., Zhong, C., Xue, T., Wang, H., Feng, Y., et al. 2012. Altered topological patterns of brain networks in mild cognitive impairment and Alzheimer's disease: a resting-state fMRI study. Psychiatry Res. Neuroimaging 202 (2), 118–125.
Martens, H., Martens, M., 2000. Modified jack-knife estimation of parameter uncertainty in bilinear modelling by partial least squares regression (PLSR). Food Qual. Prefer. 11 (1), 5–16.
McIntosh, A., Bookstein, F., Haxby, J.V., Grady, C., Meskaldji, D.-E., Fischi-Gomez, E., Griffa, A., Hagmann, P., Morgenthaler, S., Thiran, J.-P., 1996. Spatial pattern analysis of functional brain images using partial least squares. Neuroimage 3 (3), 143–157.
Fischi-Gomez, E.and Griffa, A., Meskaldji, D.-E., Hagmann, P., Morgenthaler, S., Thiran, J.-P., 2013. Comparing connectomes across subjects and populations at different scales. Neuroimage 80 (0), 416–425. Mapping the Connectome.
Meskaldji, D.-E., Morgenthaler, S., Van De Ville, D., 2015a. Functional brain connectivity evaluated by an effective and more sufficient estimator based on extreme events. Traitement Du Signal, GRETSI.
Meskaldji, D.-E., Morgenthaler, S., Van De Ville, D., 2015b. New measures of brain functional connectivity by temporal analysis of extreme events. Proceedings of the Twelfth IEEE International Symposium on Biomedical Imaging: From Nano to Macro (ISBI'15). pp. 26–29.
Meskaldji, D.-E., Morgenthaler, S., Van De Ville, D., 2015c. Statistical methods for comparing brain connectomes at different scales. SPIE Optical Engineering+ Applications. International Society for Optics and Photonics., pp. 95971L.
Meskaldji, D.-E., Preti, M.G., Bolton, T., Montandon, M.-L., Rodriguez, C., Morgenthaler, S., Giannakopoulos, P., Haller, S., Van De Ville, D., 2016. Predicting individual scores from resting state fMRI using partial least square regression. Proceedings of the Thirteenth IEEE International Symposium on Biomedical Imaging: From Nano to Macro (ISBI'16). pp. 1311–1314.
Meskaldji, D.-E., Vasung, L., Romascano, D., Thiran, J.-P., Hagmann, P., Morgenthaler, S., Ville, D.V.D., 2015d. Improved statistical evaluation of group differences in connectomes by screening-filtering strategy with application to study maturation of brain connections between childhood and adolescence. Neuroimage 108 (0), 251–264.
Mevel, K., Landeau, B., Fouquet, M., La Joie, R., Villain, N., Mézenge, F., Perrotin, A., Eustache, F., Desgranges, B., Chételat, G., 2013. Age effect on the default mode network, inner thoughts, and cognitive abilities. Neurobiol. Aging 34 (4), 1292–1301.
Mevik, B.H., Cederkvist, H.R., 2004. Mean squared error of prediction (MSEP) estimates for principal component regression (PCR) and partial least squares regression (PLSR). J. Chemometr. 18 (9), 422–429.
Mevik, B.H., Wehrens, R., 2007. The PLS package: principal component and partial least squares regression in R. J. Stat. Softw. 18 (2), 1–24.
Millis, S.R., Malina, A.C., Bowers, D.A., Ricker, J.H., 1999. Confirmatory factor analysis of the Wechsler Memory Scale-III. J. Clin. Exp. Neuropsychol. 21 (1), 87–93.
Nguyen, D.V., Rocke, D.M., 2002. Tumor classification by partial least squares using microarray gene expression data. Bioinformatics 18 (1), 39–50.
Onoda, K., Ishihara, M., Yamaguchi, S., 2012. Decreased functional connectivity by aging is associated with cognitive decline. J. Cogn. Neurosci. 24 (11), 2186–2198.
Petersen, R.C., 2004. Mild cognitive impairment as a diagnostic entity. J. Intern. Med. 256 (3), 183–194.
Qi, Z., Wu, X., Wang, Z., Zhang, N., Dong, H., Yao, L., Li, K., 2010. Impairment and compensation coexist in amnestic MCI default mode network. Neuroimage 50 (1), 48–55.
Reitan, R., 1958. Validity of the trail making test as an indicator of organic brain damage. Percept. Mot. Skills 8, 271–276.
Richiardi, J., Eryilmaz, H., Schwartz, S., Vuilleumier, P., Van De Ville, D., 2011a. Decoding brain states from fMRI connectivity graphs. Neuroimage 56 (2), 616–626.
Richiardi, J., Eryilmaz, H., Schwartz, S., Vuilleumier, P., Van De Ville, D., 2011b. Decoding brain states from fMRI connectivity graphs. Neuroimage 56 (2), 616–626.
Richiardi, J., Gschwind, M., Simioni, S., Annoni, J.M., Greco, B., Hagmann, P., Schluep, M., Vuilleumier, P., Van De Ville, D., 2012. Classifying minimally disabled multiple sclerosis patients from resting state functional connectivity. Neuroimage 62 (3), 2021–2033.
Richiardi, J., Monsch, A.U., Haas, T., Barkhof, F., Van de Ville, D., Radü, E.W., Kressig, R.W., Haller, S., 2015. Altered cerebrovascular reactivity velocity in mild cognitive impairment and Alzheimer's disease. Neurobiol. Aging 36 (1), 33–41.
Sherman, S.M., 2007. The thalamus is more than just a relay. Curr. Opin. Neurobiol. 17 (4), 417–422.
Sherman, S.M., 2016. Thalamus plays a central role in ongoing cortical functioning. Nat. Neurosci. 16 (4), 533–541.
Smith, S.M., Vidaurre, D., Beckmann, C.F., Glasser, M.F., Jenkinson, M., Miller, K.L., Nichols, T.E., Robinson, E.C., Salimi-Khorshidi, G., Woolrich, M.W., Barch, D.M., Ugurbil, K., Essen, D.C.V., 2013. Functional connectomics from resting-state fMRI. Trends Cogn. Sci. 17 (12), 666–682.
F"orstl, H., Sorg, C., Riedl, V., Calhoun, V.D., Eichele, T., Drzezga, A., Kurz, A., Zimmer, C., et al. 2007. Selective changes of resting-state networks in individuals at risk for Alzheimer's disease. Proc. Natl. Acad. Sci. 104 (47), 18760–18765.
Sporns, O., 2011. Networks of the Brain. MIT Press, Cambridge.
Tagliazucchi, E., Balenzuela, P., Fraiman, D., Chialvo, D.R., 2012. Criticality in large-scale brain fMRI dynamics unveiled by a novel point process analysis. Front. Physiol. 3, 15.
Terry, D.P., Sabatinelli, D., Puente, A.N., Lazar, N.A., Miller, L.S., 2015. A meta-analysis of fmri activation differences during episodic memory in Alzheimer's disease and mild cognitive impairment. J. Neuroimaging.
Tibshirani, R., 1996. Regression shrinkage and selection via the lasso. J. R. Stat. Soc. Ser. B Methodol. 58 (1), 267–288.
Touroutoglou, A., Andreano, J.M., Barrett, L.F., Dickerson, B.C., 2015. Brain network connectivity- behavioral relationships exhibit trait-like properties: evidence from hippocampal connectivity and memory. Hippocampus.
Tzourio-Mazoyer, N., Landeau, B., Papathanassiou, D., Crivello, F., Etard, O., Delcroix, N., Mazoyer, B., Joliot, M., 2002. Automated anatomical labeling of activations in {SPM} using a macroscopic anatomical parcellation of the {MNI}{MRI} single-subject brain. Neuroimage 15 (1), 273–289.
Van der Linden, M., Adam, S., 2004. L'épreuve De Rappel Libre/Rappel Indicé à 16 Items (RL/RI - 16), in L'é Valuation Des Troubles De La MéMoire: PréSentation De Quatre Tests De MéMoire éPisodique (Avec Leur éTalonnage). Groupe de Boeck.
Wang, L., LaViolette, P., O'Keefe, K., Putcha, D., Bakkour, A., Van Dijk, K.R., Pihlajamäki, M., Dickerson, B.C., Sperling, R.A., 2010a. Intrinsic connectivity between the hippocampus and posteromedial cortex predicts memory performance in cognitively intact older individuals. Neuroimage 51 (2), 910–917.
Wang, L., Negreira, A., LaViolette, P., Bakkour, A., Sperling, R.A., Dickerson, B.C., 2010b. Intrinsic interhemispheric hippocampal functional connectivity predicts individual differences in memory performance ability. Hippocampus 20 (3), 345–351.
Wang, Z., Jia, X., Liang, P., Qi, Z., Yang, Y., Zhou, W., Li, K., 2012a. Changes in thalamus connectivity in mild cognitive impairment: evidence from resting state fMRI. Eur. J. Radiol. 81 (2), 277–285.
Wang, Z., Liang, P., Jia, X., Jin, G., Song, H., Han, Y., Lu, J., Li, K., 2012b. The baseline and longitudinal changes of PCC connectivity in mild cognitive impairment: a combined structure and resting-state fMRI study. PloS one 7 (5), e36838.
Wang, Z., Liang, P., Jia, X., Qi, Z., Yu, L., Yang, Y., Zhou, W., Lu, J., Li, K., 2011. Baseline and longitudinal patterns of hippocampal connectivity in mild cognitive impairment: evidence from resting state fMRI. J. Neurol. Sci. 309 (1), 79–85.
Wee, C.Y., Yang, S., Yap, P.T., Shen, D., Initiative, A.D.N., et al. 2015. Sparse temporally dynamic resting-state functional connectivity networks for early MCI identification. Brain Imaging Behav. 1–15.
Wee, C.Y., Yap, P.T., Denny, K., Browndyke, J.N., Potter, G.G., Welsh-Bohmer, K.A., Wang, L., Shen, D., 2012. Resting-state multi-spectrum functional connectivity networks for identification of MCI patients. PloS one 7 (5), e37828.
Welsh, K.A., Butters, N., Mohs, R.C., Beekly, D., Edland, S., Fillenbaum, G., Heyman, A.,

1994. The consortium to establish a registry for Alzheimer's disease (CERAD). Part V. A normative study of the neuropsychological battery. Neurology 44 (4), 609.
Xia, M., Wang, J., He, Y., 2013. Brainnet viewer: a network visualization tool for human brain connectomics. PLoS ONE 8 (7), e68910.
Yamashita, M., Kawato, M., Imamizu, H., 2015. Predicting learning plateau of working memory from whole-brain intrinsic network connectivity patterns. Sci. Report. 5.
Yao, Z., Zhang, Y., Lin, L., Zhou, Y., Xu, C., Jiang, T., et al. 2010. Abnormal cortical networks in mild cognitive impairment and Alzheimer's disease. PLoS Comput Biol 6 (11) e1001006,
Yeo, B.T., Krienen, F.M., Sepulcre, J., Sabuncu, M.R., Lashkari, D., Hollinshead, M., Roffman, J.L., Smoller, J.W., Zöllei, L., Polimeni, J.R., et al. 2011. The organization of the human cerebral cortex estimated by intrinsic functional connectivity. J. Neurol. 106 (3), 1125–1165.
Yi, L., Wang, J., Jia, L., Zhao, Z., Lu, J., Li, K., Jia, J., He, Y., Jiang, C., Han, Y., 2012. Structural and functional changes in subcortical vascular mild cognitive impairment: a combined voxel-based morphometry and resting-state fMRI study.
Yue, C., Wu, D., Bai, F., Shi, Y., Yu, H., Xie, C., Zhang, Z., 2015. State-based functional connectivity changes associate with cognitive decline in amnestic mild cognitive impairment subjects. Behav. Brain Res. 288, 94–102.
Zhang, X., Hu, B., Ma, X., Xu, L., 2015a. Resting-state whole-brain functional connectivity networks for MCI classification using l2-regularized logistic regression. IEEE Trans. NanoBiosci. 14 (2), 237–247.
Zhang, Z., Liu, Y., Jiang, T., Zhou, B., An, N., Dai, H., Wang, P., Niu, Y., Wang, L., Zhang, X., 2012. Altered spontaneous activity in Alzheimer's disease and mild cognitive impairment revealed by regional homogeneity. Neuroimage 59 (2), 1429–1440.
Zhang, Z., Zheng, H., Liang, K., Wang, H., Kong, S., Hu, J., Wu, F., Sun, G., 2015b. Functional degeneration in dorsal and ventral attention systems in amnestic mild cognitive impairment and Alzheimer's disease: an fMRI study. Neurosci. Lett. 585, 160–165.
Zigmond, A.S., Snaith, R.P., et al. 1983. The hospital anxiety and depression scale. Acta Psychiatr Scand 67 (6), 361–370.